RSC Advances

ROYAL SOCIETY OF CHEMISTRY

www.rsc.org/advances

Cite this: DOI: 10.1039/c0xx00000x

www.rsc.org/xxxxxx

ARTICLE TYPE

Enhanced the light-harvesting and charge transport property of polymer solar cells by embedding $NaLuF_4$:Yb,Tm nanorods

Xinyuan Zhang [a], Kezhi Zheng [a], Chunyu Liu [a],Hao Li [a],Zhiqi Li [b],Jinfeng Li [b],Yeyuan He [b], Wenbin Guo [a,*1],Liang Shen [a] and Shengping Ruan [b*].

Received (in XXX, XXX) XthXXXXXXXXX 20XX, Accepted Xth XXXXXXXXX 20XX
DOI: 10.1039/b000000x

In this contribution, we study the effects of $NaLuF_4$:Yb,Tm nanorods (NRs) dopant on the performance of inverted polymer bulk heterojunction (BHJ) solar cells. The study allows us to investigate the impact of NRs on the light-harvesting and photocurrent in BHJ solar cells fabricated with PCDTBT blended with [6,6]-phenyl-C71-butyric acid methylester ($PC_{71}BM$) acceptor. By controlling the doping concentration, we demonstrate the power conversion efficiency (PCE) of PCDTBT: $PC_{71}BM$ solar cells increases from 6.02% to 7.18% mainly due to improving light absorption and photocurrent. The single carrier devices reveal that the electron and hole mobilities both rise in doped devices, contributing to the enhancement of photoconductivity and consequent PCEs.

1. Introduction

As a result of the use of low-cost materials, ease of processing, and rapid increase in power conversion efficiencies (PCE), solution-processed bulk heterojunction (BHJ) polymer solar cells (PSCs) have attracted considerable attention as a potentially practical approach to solar energy harvesting.[1-3] PSCs efficiency has been reached over 10%, which has been a promising alternative to conventional inorganic photovoltaic devices.[4-8] Compared with their inorganic counterparts, the PSCs efficiency is still lower, and further improvements are necessary to make PSCs commercially viable. The efficiency of PSCs is limited by a few factors, such as low light-trapping, unsatisfactory excition migration and dissociation, charge transport, and charge recombination, which are significantly influenced by the active layer films. Typically, the active layer of PSCs involves a phase-separated blend of an electron-donating conjugated polymer and an electron-accepting fullerene derivative.[9-11] Tremendous efforts have been made to optimize the active layer formation and the device configuration,[12,13] such as different solvents doping, thermal annealing of the active layer, optical spacer adding, and tandem structure, which have obtained effective improvement in PSCs performance. [14-22]

As we know, about 52% of total solar energy flux is in the infrared (IR) and near-infrared (NIR) range, so the utmost using of the NIR part of the solar radiation is a practical method to further enhance the performance of solar cells. Highly efficient solar cells require absorbing photons over the possibly broad range of the solar spectrum followed by effective generation and collection of charge carriers. One widely adopted strategy to enhance the number of absorbed photons and resultant photocurrent is by decreasing the optical band gap of the active layer to achieve a better absorption overlap with the solar spectrum. Up-conversion (UC) is a luminescence of transforming two or more low-energy photons into one high-energy photon.[23-29] UC is a smart concept to exploit the IR and NIR photons, which may enhance the response of solar cells in the IR region. A great deal of work has been done to utilize inorganic nanoparticles (NPs) including UC effect to enlarge the absorption coefficient of active materials in polymer solar cells.[30,31] In addition, incorporation of NPs with UC function into the solar cell devices can not only increase light trapping of active layer but also apparently improve charge transport properties.[32-35] Meanwhile, The NPs can play a role as light-scattering centers and tune the morphology of active layer. Lanthanide Rare-earth ions, such as $NaLuF_4$ and $NaYF_4$ possess superior UC efficiency, have been used in optoelectronic devices to enhance light capture in NIR region and improve charge transport and charge injection. In this paper, the cubic phase $NaLuF_4$:Yb,Tm nanorods (NRs) were prepared by a facile solvo thermal approach and introduced into active layer of PSCs. The NRs have an average size of ~50 nm and can be well dispersed in the blend solution. The performances of PSCs fabricated with different doping concentration are investigated and compared.

2. Experimental

2.1 Material preparation:

$LnCl_3$ (Ln = Lu, Yb, and Tm, 99.999%) compounds were purchased from Shanghai Shabo Chemical Technology Company. Oleic acid (OA) and 1-octadecene (ODE) were obtained from Alfa Aesar. Oleylamine (OM) and sodium oleate (NaOA) were obtained from Aladdin. Ammonium fluoride (NH_4F) with A.R purity was bought from Beijing Fine Chemical Company, China.

Cite this: DOI: 10.1039/c0xx00000x

www.rsc.org/xxxxxx

ARTICLE TYPE

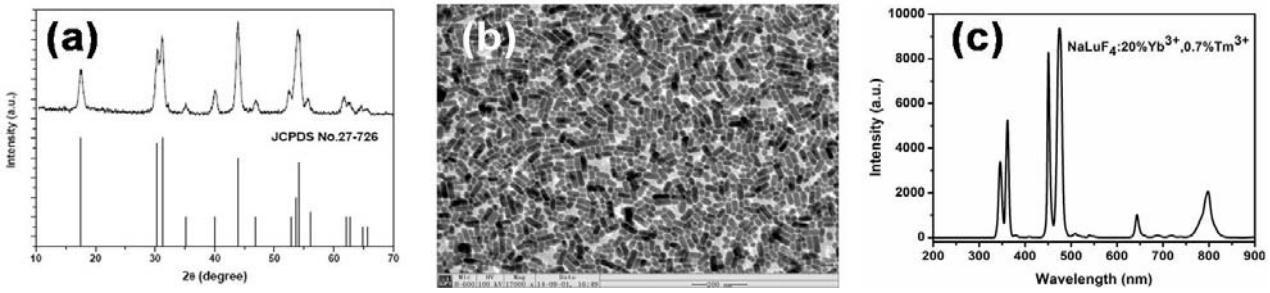

Fig.1 (a) XRD image, (b) TEM image, and (c) up-conversion emission spectrum of $NaLuF_4$:Yb, Tm crystals.

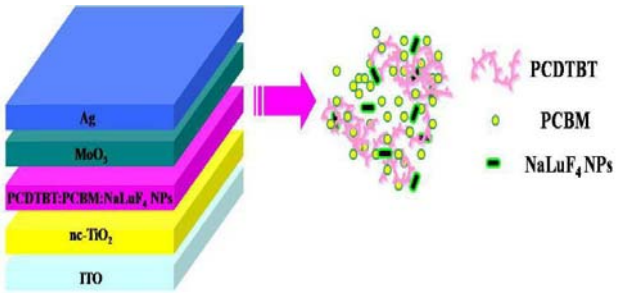

Fig.2 The device structure of the inverted polymer solar cells based on $NaLuF_4$:Yb, Tm NRs doping.

All other chemicals were analytical grade and used without further purification.

A typical procedure for the synthesis of β-$NaLuF_4$:20%Yb, 0.7%Tm is as follows: 1 mmol $LnCl_3$ (Ln = Lu, Yb, and Tm) was added to a 100 mL three-necked flask containing a certain amount of OA, OM and ODE. The solution was stirred and heated at 110 °C for 1 h under vacuum. The solution was then cooled to room temperature using a gentle flow of argon gas. Solid NaOA and anhydrous NH_4F were added to the flask, and the mixed solution was then heated at 320 °C for 1 h. When the solution had cooled to room temperature, solid state products were precipitated with 50 mL of ethanol, then collected after centrifugation, washed with ethanol twice, and finally redispersed in methylbenzene for further experiments. X-ray diffraction (XRD) analysis of $NaLuF_4$:Yb, Tm powder was carried out with a powder diffractometer (Model Rigaku RU-200b), using Ni-filtered Cu Kα radiation (λ=1.5406 Å) with 200 mA current and 50 kV voltage across the tube to generate powerful X-rays. The XRD measurement was performed at a scan rate of 18^o min^{-1} and step size of 0.02^o. Fig.1(a) exhibits that $NaLuF_4$:Yb,Tm is hexagonal phase. Fig.1(b) shows the transmission electron microscope (TEM) images of synthesized cubic phase $NaLuF_4$:Yb, Tm crystals, in which we can see that $NaLuF_4$:Yb, Tm NRs are 50 nm in length and 15 nm in diameter on average. Fig.1(c) is the up-conversion emission spectrum $NaLuF_4$:Yb, Tm NRs, and the emission peaks are located in 360 nm and 470 nm. In Yb^{3+}-Tm^{3+} codoped systems, Yb^{3+} ions absorb pumping photons and successively transfer energy to Tm^{3+} to populate their $^3H_5$, $^3F_{3,2}$, and $^1G_4$ levels in turn. The $^1D_2$ state is populated through the cross relaxation $^3F_3 \rightarrow {}^3H_6$: $^3F_3 \rightarrow {}^1D_2$ (Tm^{3+}) due to the large energy mismatch (~3500 cm^{-1}) between $^1G_4$ and $^1D_2$, which cannot be directly populated by the ET $^2F_{5/2} \rightarrow {}^2F_{7/2}$ (Yb^{3+}) : $^1G_4 \rightarrow {}^1D_2$ (Tm^{3+}). The $^3P_2$ level of Tm^{3+} is populated by the ET $^2F_{5/2} \rightarrow {}^2F_{7/2}$ (Yb^{3+}): $^1D_2 \rightarrow {}^3P_2$ (Tm^{3+}) and then relaxes rapidly to the $^1I_6$ level.[36-40]

2.2 Device fabrication and characterization

β-$NaLuF_4$:20%Yb, 0.7%Tm NRs was dissolved in toluene solution and concentration is 1 mg mL^{-1}.The device structure is shown in Fig.2. The invert OSC devices have a configuration of indium tin oxide (ITO)/titanium dioxide (TiO_2) (25 nm)/active layer (100 nm)/ molybdenum oxide (MoO_3)（10 nm）/sliver (Ag) (100 nm). The nc-TiO_2 film covered on the ITO act as an electron-selective layer, while MoO_3 high work function (-5.9 eV) at the photoactive layer/Ag interface will enhance hole collection.[41-44]Patterned ITO-coated glass substrates were sonicated consecutively with acetone, isopropyl alcohol, and deionized water for 10 min and subsequently dried with nitrogen. Anatase TiO_2 layer was prepared onto ITO substrate and the thin film was then thermally annealed at 450 ℃ for 2 h in the muffle furnace. For the active layer, the1,2-dichlorobenzene (DCB) solution composed of PCDTBT(7 $mgmL^{-1}$),$PC_{71}BM$(28 $mgmL^{-1}$) and were doped with 0,10μL, 20μL, 30μL, 40μL $NaLuF_4$:20%Yb, 0.7%Tm NRs solution, respectively. The corresponding weight ratio (wt) of NRs and PCDTBT:$PC_{71}BM$ are 0, 0.029wt%, 0.058wt%, 0.087wt%, 0.116wt%. Accordingly, different doping devices are named as Device A, Device B, Device C, Device D, and Device E. Poly-[N-9''-hepta-decanyl-2,7-carbazolealt-5,5-(40,70-di-2-thienyl-20,10,30ben-zothia–diazole)] (PCDTBT) is electron donor and fullerene derivative [6,6]-phenyl-C_{71}-butyric acid methylester ($PC_{71}BM$) is acceptor. The blend solution was spin-cast at 2000 RPM on top of the nc-TiO_2 layer in air, and the thickness of active layer is about 100 nm. The samples with PCDTBT:$PC_{71}BM$ were baked in the atmosphere of argon in the glove box at 70 ℃ for 20 min. Finally, the devices were completedby thermal evaporation of MoO_3 and Ag electrode under a base vacuum of 5.0×10^{-4} Pa. The active area of the inverted devices was about 0.064 cm^2.

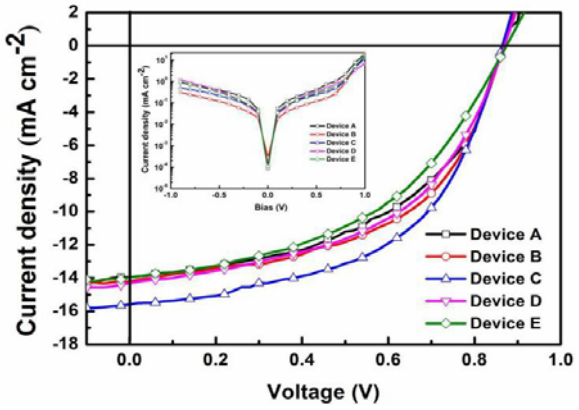

Fig.3 *J-V* characteristics of the devices with different amount of NRs under AM 1.5G illumination with an intensity of 100 mW cm^{-2} in ambient air, inset is *J-V* characteristics of devices with different doping amount of NRs in dark.

Current density-voltage(*J-V*) characteristics were measured with a computer-programmed Keithley 2400 source/meter under AM1.5G solar illuminations with an Oriel 300 W solar simulator intensity of100 $mWcm^{-2}$ (about one sun) in air without encapsulation. The light intensity was measured with a photometer (Internationallight, IL1400) corrected by a standard silicon solar cell. The incident photon-to-current efficiency (IPCE) was measured with Crowntech QTest Station 1000 AD. The absorption and transmittance spectra were measured by means of ultraviolet/visible spectrometer (UV 1700, Shimadzu).

3. Result and discussion

The *J-V* characteristics of all finished devices are shown in Fig.3 The device A without NRs doping exhibits a short circuit current density (J_{sc}) of 13.946 mA cm^{-2}, open-circuit voltage (V_{oc}) of 0.867 V and fill factor (FF) of 49.8%, leading a PCE of 6.022%. As expected, the performance of devices C has been apparently improved, the PCE of device C made with an optimal doping amount of 0.058wt% is 7.175%, with a J_{sc} of 15.585 mA cm^{-2}, V_{oc} of 0.865 V and FF of 53.24%. J_{sc} and FF are both improved, J_{sc} rises from 13.946 mA cm^{-2} to15.585 mA cm^{-2} and FF rises from 49.8% to 53.24%, which directly brings an 19% enhancement of PCE than device A.

Meanwhile, the device B and D were also conducted, and they demonstrate relatively higher PCE than contrast device. The detailed results are summarized in Table I, and the values are typical average of 50 devices. Noticeably, V_{oc} remained the same level as that of the reference device, which suggests that the $NaLuF_4$:20%Yb, 0.7%TmNRs have no large influence on the energy level distribution of the devices. It is widely believed that the V_{oc} mainly originates from the energy difference between the highest occupied molecular orbital (HOMO) of donor and the lowest unoccupied molecular orbital (LUMO) of acceptor. [45,46] In addition, device E with doping amount of 0.116wt% NRs shows apoor performance especially in FF compared with other devices. The excess NRs doping is adverse to the quality of the film of active layer, which might result in a poor phase separation and then decrease exciton dissociation and charge mobility. The inset of Fig.3 shows the dark *J-V* curves of control and doped devices in the absence of illumination. The doped devices show smaller leakage current at negative voltages. Meanwhile, higher current in the space charge limited current dominated regime was achieved for doped devices, indicating an increase of charge transfer speed and a decrease of series or contact resistance, which will produce a well rectifying effect compared with contrast devices. [47]

Table I Device performance, including open-circuit voltage (V_{oc}),short-circuit current density (J_{sc}), fill factor (FF), power conversion efficiency (PCE), series resistance (R_s) and shunt resistance (R_{sh}) of devices in our study.

Device	V_{oc} (V)	J_{sc} (mA cm^{-2})	FF (%)	PCE (%)	R_s (ohm)	R_{sh} (ohm)
A	0.867	13.946	49.80	6.022	322.646	4348.32
B	0.867	14.199	52.62	6.478	179.967	4093.80
C	0.865	15.585	53.24	7.175	180.211	4416.98
D	0.869	14.316	50.33	6.236	220.150	3462.04
E	0.874	13.949	46.75	5.699	344.285	3839.60

In order to further understand the effect of $NaLuF_4$:Yb, Tm NRs, another control experiment was performed by simply adding $NaLuF_4$ (0.058wt%) NRs into PCDTBT:$PC_{71}BM$ solution without Yb and Tm ions (Fig. 4). The result shows that the J_{sc} and PCE of the device with $NaLuF_4$ NRs are both higher than that of the undoped devices, lower than that of doped cells. This indicates that doped $NaLuF_4$ and $NaLuF_4$:Yb,Tm into active layer of PSCs can both improve the performance of cells, but the device performance of doped $NaLuF_4$:Yb, Tm are much higher, which is attributed to the UC of Yb and Tm ions. Why the properties of cells doped $NaLuF_4$ NRs was also higher than that of control devices. The following possible factors may illustrate the effect of $NaLuF_4$ NRs. Firstly, the optical path length in the active layer can be increased because of scattering of $NaLuF_4$ NRs. Secondly, the near field will extend into the active layer at a large extent, and the possibility of interaction coupling between the near field and the incident light will be enhanced, improving the photo-generation of excitons of active layer. [48-50]

The incident photon-to-current efficiency (IPCE) spectra of all devices are shown in Fig.5. The IPCE of the device A shows a maximum of 62% at 525 nm. When incorporating 0.058wt% NRs, the IPCE of Device C shows a maximum of 69.5% at 475 nm, a little higher than that of Device A. This is consistent with the data from *J–V* curves. IPCE of devices doped with NRs are apparently improved from 350 nm to 630 nm compared with Device A. As shown in Fig. 1(b), the emission peaks of $NaLuF_4$:Yb,Tm are in Fig.1(b), the emission peaks of $NaLuF_4$:Yb,Tm are located in 360 nm and 470 nm, which probably contributes to the enhancement of IPCE. Fig. 6(a) is light-harvesting spectrum of active layer film with and without doping NRs. It can be seen that light harvesting of doped film got modestly increase. Fig. 6(b) is the light transmittance spectra of active layers with different ratios of NRs, which is corresponding with Fig. 6(a). The enhanced light trapping in the NRs doped devices can be attributed to the increase of light path from the scattering of cubic phase $NaLuF_4$ NRs, and UC effect deriving from Yb^{3+} and Tm^{3+} ions also make a contribution to improve light absorption.

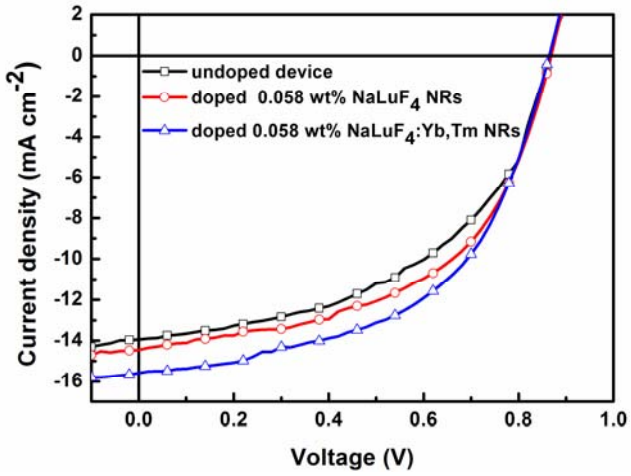

Fig.4 *J-V* characteristics comparison of cells without doping, doped with 0.058wt% $NaLuF_4$ NRs, and doped with 0.058wt%$NaLuF_4$:Yb, Tm NRs.

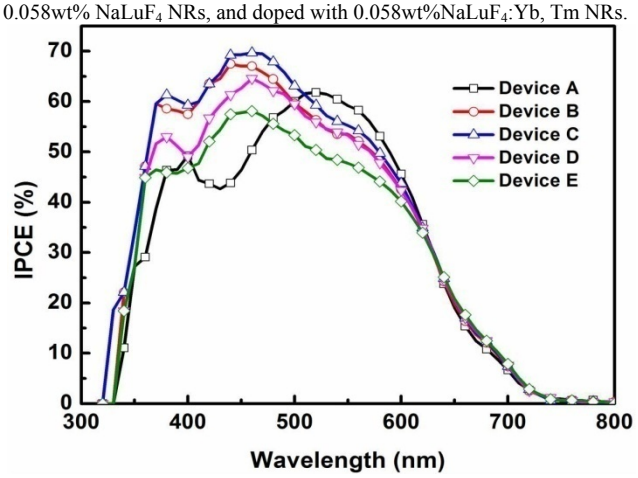

Fig.5 (a) The absorption spectra of the active layers with different doping amount of NRs, inset is absorption spectrum from 600 nm to 750 nm, (b) The transportation spectra of the devices with different doping amount of NRs, inset is transmittance spectrum from 600 nm to 750 nm.

In order to investigate the role of NRs on charge transport properties, we fabricated two kinds of single carrier devices. The hole-only device configuration is ITO/MoO_3/active layer/MoO_3/Ag, the MoO_3 connected with ITO is electron blocking layer. The 2,9-dimethyl-4,7-diphenyl-1,10-phenanthroline (BCP) is used as hole blocking layer, and the electron-only device configuration is ITO/TiO_2/active layer/BCP/Ag. The *J-V* characteristics in dark of these two kinds of devices were shown in Fig.7. We observe that J_{sc} of doped devices has been mildly enhanced respective of doping amount in both the hole-only devices and the electron-only devices. According to the data of Fig.7, charge carrier mobilities were calculated from Mott-Gurney law, including field dependence. It will apply a realistic evaluation on the apparent charge carrier mobility in the active layer according to *J-V* characteristics of single charge carrier devices. At a typical applied voltage of 5.0 V, corresponding to an electric field of 5×10^5 V cm^{-1} across the bulk of a 100 nm device, apparent hole mobilities of 7.52×10^{-5} $cm^2V^{-1}s^{-1}$,8.78×10^{-5} $cm^2V^{-1}s^{-1}$, 1.19×10^{-4} $cm^2V^{-1}s^{-1}$, 8.67×10^{-5} $cm^2V^{-1}s^{-1}$, and 8.53×10^{-5} $cm^2V^{-1}s^{-1}$, and apparent electron mobilities of 3.22×10^{-4} $cm^2V^{-1}s^{-1}$, 5.67×10^{-4} $cm^2V^{-1}s^{-1}$,7.85×10^{-4} $cm^2V^{-1}s^{-1}$, 5.96×10^{-4} $cm^2V^{-1}s^{-1}$, and 4.17×10^{-4} $cm^2V^{-1}s^{-1}$ have been

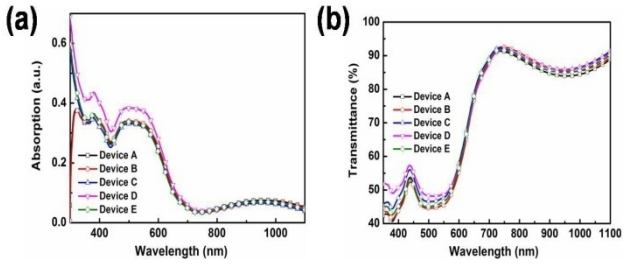

Fig.6 (a) The absorption spectra of the active layers with different doping amount of NRs, (b) The transmittance spectra of the devices with different doping amount of NRs.

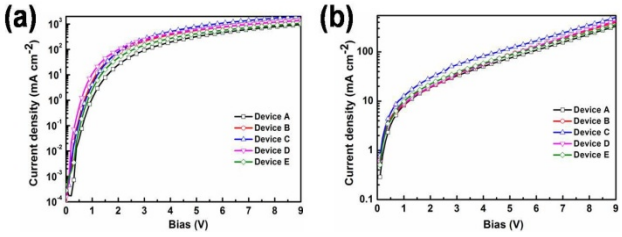

Fig.7 *J-V* characteristics of single carrier device in dark (a) electron-only device and (b) hole-only device.

determined for the Devices A and Devices B, C, D, E, respectively. Both the hole and electron mobilities were increased and a more balanced charge transport in doped devices can be achieved. This indicates incorporating NRs into active layer is benefit to increase exciton dissociation and enhance carriers transport properties thus increasing the J_{sc} of devices. Simultaneously, we obtain a largest J_{sc} with 0.058wt% NRs doping, which is consistent with the tendency of the photocurrent in Fig.3, suggesting that the charge transport properties are substantially improved. To investigate the impact of NRs on the interface resistance of devices, the impedance spectra of all devices were measured with frequency of 20 to 1 MHz, and the results are shown in Fig.8. The semicircle's diameter in the diagram stands for the impedance. In other words, the larger diameter means larger impedance. It indicates that the semicircle's diameter of devices doped with NRs are smaller than control devices. Thus, the additive of NRs brings significant decline to the devices impedance, which explains the increase of the J_{sc}.

The surface morphology of active layer is very important to the photovoltaic performance of polymer BHJ solar cells. Fig.9 shows the surface morphology of active layers of Device A, Device B, Device C, and Device D in AFM (atom force microscopy) images. Their surfaces are quite smooth and the root-mean-square (RMS) roughness of the four active layers is 0.36 nm, 0.48 nm, 0.54 nm, and 0.66 nm, respectively. The doped and undoped films have similar surface morphologies, while doped films have a higher RMS. According to the BHJ solar cell model, the V_{oc} is determined by the energy difference between HOMO level of the donor and the LUMO level of the acceptor and little influenced by the film morphology, so V_{oc} is almost same for all devices. It has been well acknowledged that continuous interpenetrating networks with proper domain size are essential for the efficient exciton separation and charge transport,

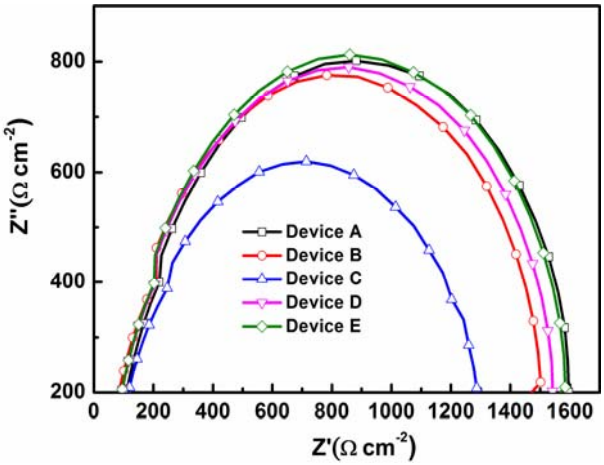

Fig.8 The complex impedance characteristics of all devices.

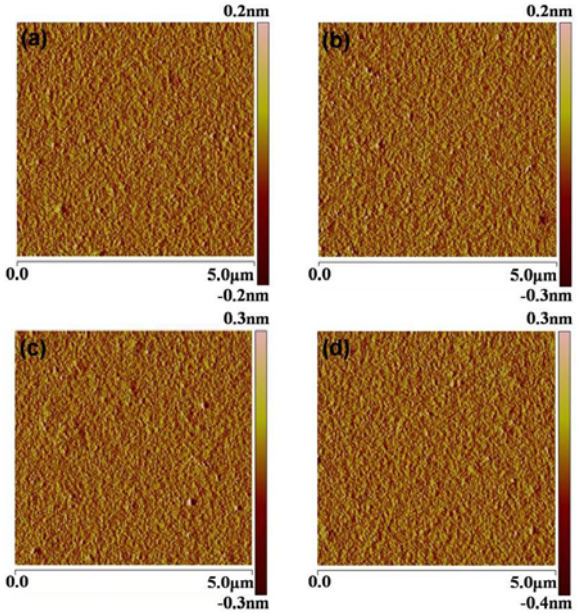

Fig.9 AFM images of PCDTBT:$PC_{71}BM$ film without and with different ratios NRs.

which are key factors to enhance the J_{sc} and FF. Comparison of the AFM images of all active layers indicates that the higher RMS roughness of doped films leads to higher J_{sc} and FF, which is consistent with the *J-V* characteristics shown in Fig.3.

4. Conclusion

In conclusion, we have investigated the role of $NaLuF_4$:Yb,Tm NRs dispersed into the active layer on the performance of inverted BHJ OSCs based on PCDTBT:$PC_{71}BM$ blending. Compared with the reference device without NRs, the maximum 19% enhancement in power conversion efficiency (from 6.022 % to 7.175 %) was achieved. And increasing J_{sc} 、 FF and unchangeable V_{oc} were observed in the devices containing the NRs with optimized doping amount of 0.058wt%. The evaluations of device photovoltaic characteristics demonstrated that the generation rate and the dissociation probability of excitons were improved after introducing NRs, resulting in improved J_{sc} and FF. The introduction of $NaLuF_4$ NRs can not only increase the optical path length as scattering center, but also can convert IR and NIR photons into visible photons and thus increases the light harvesting of active layer, leading to a higher PCE.

Acknowledgements

Supported by National Natural Science Foundation (Grant Nos. 61275035, 61274068, 61077046), Chinese National Programs for High Technology Research and Development (Grant No. 2013AA030902), Doctoral Found of Ministry of Education of China (Grant Nos.20100061120045 and 20110061130004), Project of Science and Technology Development Plan of Jilin Province (Grant Nos. 20130206075SF, 20110314, 20120324), the Opened Fund of the State Key Laboratory on Integrated Optoelectronics (No. IOSKL2012KF03).

Notes and references

a. State Key Laboratory on Integrated Optoelectronics, Jilin University, 2699 Qianjin Street, Changchun 130012, People's Republic of China
b. College of Electronic Science and Engineering, Jilin University, 2699 Qianjin Street, Changchun 130012, People's Republic of China

1 J.Y. Kim, K. Lee, N.E. Coates, D. Moses, T.Q. Nguyen, M. Dante, A. J. Heeger, Science , 2007, **317**,222.
2 F.C. Krebs, H. Spanggard, T. Kjær, M. Biancardo, J. Alstrup, Mater. Sci. Eng. B , 2007, **138**,106.
3 L. Blankenburg, K. Schultheis, H. Schache, S. Sensfuss, M. Schrödner, Sol. Energy Mater. Sol. Cells, 2009, **93**,476 .
4 F. C. Krebs, Sol. Energy Mater. Sol. Cells , 2009, **93**,1636.
5 F. C. Krebs, Organic Electronics , 2009, **10**, 761.
6 F. C. Krebs, M. Jorgensen, K. Norrman, O. Hagemann, J. Alstrup, T. D. Nielsen, J. Fyenbo, K. Larsen, J. Kristensen, Sol. Energy Mater. Sol. Cells, 2009, **93**, 422.
7 F. C. Krebs, Sol. Energy Mater. Sol. Cells, 2009,**93**, 465.
8 F. C. Krebs, Sol. Energy Mater. Sol. Cells , 2009, **93,**394.
9 C. Edwards, A. Arbabi, G. Popescu and L. L. Goddard, Light Sci. Appl. , 2012, **1**e30.
10 S. E. Shaheen, C. J. Brabec, N. S. Sariciftci, F. Padinger, T. Fromherz, J. C. Hummelen, Appl. Phys. Lett.,2001, **78**, 841.
11 M. T. Rispens, A. Meetsma, R. Rittberger, C. J. Brabec, N. S. Sariciftci, J. C. Hummelen, Chem. Commun. , 2003, **17**, 3116.
12 M. D. Irwin, D. B. Buchholz, A. W. Hains, R. P. H. Chang, T. J. Marks, Proc. Nat. Acad. Sci. , 2008, **105**, 2783.
13 R. Steim, S. A. Choulis, P. Schilinsky, C. J. Brabec, Appl. Phys.Lett. , 2008, **92**, 093303.
14 S. E. Shaheen, C. J. Brabec, N. S. Sariciftci, Appl. Phys. Lett. , 2001, **78**, 841.
15 F. Padinger, R. S. Rittberger, N. S. Sariciftci, Adv. Funct. Mater. , 2003, **13**,85.
16 R. A. Taylor, T. Otanicar and G. Rosengarten, Light Sci. Appl. , 2012, **1**,e34.
17 C. Xiang, W. Koo, F. So, H. Sasabe, J. Kido, Light Sci. Appl. , 2013, **2**, e74.
18 W. Ma, C. Y. Yang, X. Gong, K. Lee, A. J. Heeger, Adv. Funct. Mater., 2005,**15**, 1617.
19 J. Y. Kim, K. Lee, N. E. Coates, D. Mose, T. Q. Nguyen, M. Dante, A. J. Heeger, Science , 2007, **317**, 222.
20 S. H. Park, A. Roy, S. Beaupre, S. Cho, N. Coates, J. S. Moon, D. Moses, M. Leclerc, K. Lee, A. J. Heeger, Nature Photonics , 2009, **3**, 297.

21 J .Perez-Juste, I. Pastoriza-Santos, L. M. Liz-Marzan, Coordin Chem. Rev , 2005,**249**, 1870.

22 D. H. Wang, D. Y. Kim, K. W. Choi, J. H. Seo, S. H. Im, J. H. Park, O. Park, A. J. Heeger, Angew. Chem. , 2011,**50**, 5633.

23 C. F. Guo, T. S. Sun, F. Cao, Q. Liu, Z. F. Ren, Light Sci. Appl., 2014,**3**, e161.

24 L. L. Huang, X. Z. Chen, B. F. Bai, Q. F. Tan, G. F. Jin, T. Zentgraf, S. Zhang, Light Sci. Appl. , 2013, **2**, e70.

25 X. Chen, B. H. Jia, Y. A. Zhang, M. Gu, Light Sci. Appl. , 2013, **2**, e92.

26 Z. Holman, S. Wolf, C. Ballif, Light Sci. Appl., 2013, **2**, e106.

27 J. de Wild, J. K. Rath, A. Meijerink, W. G. J. H. M. Van Sark, R. E. I. Schropp, Sol. Energy Mater. Sol. Cells , 2010, **94**, 2395.

28 T. Trupke, A. Shalav, B. S. Richards, P. Wurfel, M. A. Green, Sol. Energy Mater. Sol. Cells, 2006, **90**, 3327.

29 T. Trupke, M. A. Green, P. Wurfel, J. Appl. Phys., 2002, **92**, 4117.

30 A. Shalav, B. S. Richards, T. Trupke, Appl. Phys. Lett., 2005,**86**, 013505.

31 B. S. Richards , Sol. Energy Mater. Sol. Cells , 2006, **90**, 1189.

32 C. W. Lin, D. Y. Wang, Y. T. Wang, C. C. Chen, Y. J. Yang and Y. F. Chen, Sol. Energy Mater. Sol. Cells, 2011, **95**, 1107.

33 H. C. Liao, C. S. Tsao, T. H. Lin, M. H. Jao, C. M. Chuang, S. Y. Chang, Y. C. Huang, Y. T. Shao, C. Y. Chen, C. J. Su, U. S. Jeng, Y. F. Chen and W. F. Su, ACS Nano , 2012, **6**, 1657.

34 B. Paci, G. D. Spyropoulos, A. Generosi, D. Bailo, V. R. Albertini, E. Stratakis and E. Kymakis, Adv. Funct. Mater. , 2011,**21**, 3573.

35 D. H. Wang, D. Y. Kim, K. W. Choi, J. H. Seo, S. H. Im, J. H. Park, O. Ok Park and A. J. Heeger,Angew. Chem., Int. Ed. , 2011, **50**, 5519.

36 R. S. Khnayzer, J. Blumhoff, J. A. Harrington, A. Haefele, F. Deng and F. N. Castellano, Chem Comm, 2012,**48**, 209.

37 M. Zhang, Y. Lin, T. J. Mullen, W. Lin, L. D. Sun, C. H. Yan, T. E. Pattern, D. Wang and G. Liu, J. Phys. Chem. Lett.,2012, **3**, 3188.

38 J. Méndez-Ramos, P. Acosta-Mora, J. C. Ruiz-Morales, T. Hernandez, M. E. Borges and P. Esparza, RSC Adv., 2013, **3**, 23028 .

39 S. Obregón and G. Colón, Chem. Commun., 2012,**48**, 7865.

40 G.F. Wang, W.P. Qin, L.L. Wang, G.D. Wei, P.F. Zhu, and R.J. Kim, Opt. Express 2008, **16**, 11907.

41 J. Meyer, S. Hamwi, M. Kroger, W. Kowalshy, T. Riedl, A. Kahn, Adv. Mater. , 2012, **24**, 5408.

42 M. Kroger, S. Hamwi, J. Meyer, T. Riedl, W. Kowalsky, A. Kahn, Org. Electron. , 2009, **10**, 932.

43 Y. H. Su, Y. F. Ke, S. L. Cai, Q. Y. Yao, Light Sci. Appl. , 2012, **1**,e14.

44 D. Lepage, A. Jimenez, J. Beauvais, J. J. Dubowski, Light Sci. Appl. , 2012, **1**, e28.

45 G. Dennier, M. C. Scharber, T. Ameri, P. Denk, K. Forberich, C. Waldauf, C. J. Brabec, Adv. Mater. , 2008, **20**, 579.

46 M. C. Scharber, D. Wuhlbacher, M. Koppe, P. Denk, C. Waldauf. A. J. Heeger, C. J. Brabec, Adv. Mater. , 2006, **18**, 789.

47 C. Tao, S. P. Ruan, G. H. Xie, X. Z. Kong, L. Shen, F. X. Meng, C. X. Liu, X. D. Zhang, W. Dong and W. Y. Chen, Appl. Phys. Lett. , 2009, **94**,043311.

48 J. L. Wu, F. C. Chen, Y. S. Hsiao, F. C. Chien, P. Chen, C. H. Kuo, M. H. Huang, and C. S. Hsu,ACS Nano. , 2011, **5**, 959 .

49 M. Heo, H. Cho, J. W. Jung, J. R. Jeong, S. Park, and J. Y. Kim, Adv. Mater. , 2011, **23**,5689.

50 I. Kim, T. S. Lee, D. S. Jeong, W. S. Lee, and K. S. Lee, J. Phys. D: Appl. Phys. , 2012, **45**, 065101.